The impact of wintertime sea-ice anomalies on high surface heat flux events in the Iceland and Greenland Seas

James O. Pope[1,2*], Thomas J. Bracegirdle[1], Ian A. Renfrew[3], and Andrew D. Elvidge[3]

[1.] *British Antarctic Survey, Cambridge, UK*

[2] *Now at Met Office Hadley Centre, Met Office, Exeter, UK*

[3.] *School of Environmental Sciences, University of East Anglia, Norwich, UK*

* Corresponding Author: Dr James Pope (james.pope@metoffice.gov.uk), Met Office, FitzRoy Road, Exeter, Devon, EX1 3PB, UK.

Submitted to: *Climate Dynamics*

Revised Submission: 17th October 2019

Abstract

The gyres of the Iceland and Greenland Seas are regions of deep-water formation, driven by large ocean-to-atmosphere heat fluxes that have local maxima adjacent to the sea-ice edge. Recently these regions have experienced a dramatic loss of sea ice, including in winter, which begs the question have surface heat fluxes in the adjacent ocean gyres been affected? To address this a set of regional atmospheric climate model simulations has been run with prescribed sea ice and sea surface temperature fields. Three 20-year model experiments have been examined: Ice_{max}, Ice_{med} and Ice_{min}, where the surface fields are set as the year with maximum, median and minimum sea-ice extents respectively. Under conditions of reduced sea-ice extent there is a 15% (19 W m^{-2}) decrease in total wintertime heat fluxes in the Iceland Sea. In contrast, there is an 8% (9 W m^{-2}) increase in heat fluxes in the Greenland Sea primarily due to higher local SSTs. These differences are manifest as changes in the magnitude of high heat flux events (such as cold air outbreaks). In the Iceland Sea, 76% of these events are lower in magnitude during reduced sea-ice conditions. In the Greenland Sea, 93% of these events are higher in magnitude during reduced sea-ice conditions as a result of higher SSTs coincident with retreating sea ice. So, in these experiments, the reduced wintertime sea-ice conditions force a different response in the two seas. In both gyres, large-scale atmospheric circulation patterns are key drivers of high heat flux events.

Keywords: surface heat flux; sea ice; Iceland Sea; Greenland Sea; MetUM; climate modelling

1. Introduction

Between the Arctic Ocean and the North Atlantic there is a band of sub-polar seas within which warm Atlantic water is transformed into cold, dense water, which flows south as a contributor to North Atlantic Deep Water (NADW). A key component of NADW is thought to form in the Iceland and Greenland Seas and contribute to Denmark Strait Overflow Water via the East Greenland Current and the North Icelandic Jet (Våge et al. 2011; 2013; Moore et al. 2015). The East Greenland Current, fed by re-circulating Atlantic Water and Arctic-origin water masses, can also be influenced by atmosphere-ocean coupling in this region (e.g. Våge et al. 2013).

Across the Greenland, Iceland and Norwegian Seas, the largest wintertime oceanic heat loss is driven by marine cold air outbreaks (CAOs), representing 60-80% of positive wintertime heat fluxes in the North Atlantic (Papritz & Spengler 2017). Marine CAOs drive air-sea fluxes when cold, dry polar air – originating over cold land masses or sea ice – is transported over comparatively warm ice-free ocean surfaces (Kolstad 2017). Although typically less severe than the Labrador Sea (Moore et al. 2012), CAOs over the Greenland and Iceland seas are thought to have a particularly influential role in triggering ocean convection and water-mass transformations in this region (Våge et al. 2011; 2013; 2018; Renfrew et al. 2019b). Other mesoscale weather systems, such as barrier flows along the Greenland coast (e.g. Petersen et al. 2009; Harden et al. 2011) and polar mesoscale cyclones (e.g. Renfrew et al. 2008; Michel et al. 2018) also significantly enhance surface fluxes in these locations and have been shown to impact water-mass transformations (Condron and Renfrew 2013; Condron et al. 2008; Jung et al. 2014).

While marine CAOs drive air-sea fluxes, the translation of these atmosphere-ocean interactions into oceanic convection and deep water formation requires the ocean to be preconditioned (Marshall and Schott 1999). This occurs through the presence of a cyclonic gyre, which tilts the isopycnals and allows denser water to be exposed to the surface, allowing subsequent air-sea fluxes to cause a loss of buoyancy in these surface waters which can then sink to depth (Marshall and Schott 1999). Moore et al. (2015) focused on the gyres in the Iceland and Greenland Seas and estimated that air-sea heat fluxes there had reduced by 20% between 1979 and 2014. They hypothesised that this reduction was due to both the differential warming of the atmosphere and ocean, and changes in the distribution of air-sea heat fluxes associated with a reduction in wintertime sea-ice extent. Their reanalysis-based study could not distinguish between these two factors. Peak air-sea heat fluxes tend to occur immediately downwind of the marginal-ice-zone during cold air outbreaks (e.g. Brümmer 1997; Renfrew and Moore 1999). Decreases in wintertime sea-ice extent of about 10% per decade have been found for the Greenland Sea (Cavalieri and Parkinson 2012; Onarheim et al. 2018); implying that the marginal-ice-zone is retreating poleward and, consequently, the associated heat flux maximum will follow it, leading to a separation of the oceanic gyres and the greatest heat flux forcing (c.f. Moore et al. 2015). Note that cold air mass transformations have been shown by Chechin and Lüpkes (2017) to occur within 850 km of the ice edge. In short, anthropogenic warming and the wintertime retreat of sea ice suggest a change in deep water formation may be underway, which could lead to a reduction in the supply of NADW to the southward limb of the Atlantic Meridional Overturning Circulation and potentially weakening that whole circulation system (Moore et al. 2015). Proving this hypothesis requires an understanding of how these changes in sea-ice distribution will affect surface heat fluxes in the vicinity in the Iceland and Greenland Seas.

The aim of this paper is to assess how changes in sea-ice extent in the Iceland and Greenland Seas affects surface heat fluxes and high heat flux events. To achieve this, we have carried out atmosphere-only regional climate modelling with different sea ice and sea surface temperature (SST) lower boundary conditions. We quantify the climatological impact of sea-ice anomalies on surface heat fluxes, and other key surface parameters, with a focus on the Iceland and Greenland Sea gyres. The role of anthropogenic differential warming of the atmosphere and ocean is not examined.

2. Methods

2.1 Model Description

We have used the UK Met Office Unified Model (MetUM) version 10.6 with a regional nested domain to carry out a suite of simulations of the atmosphere over the NE North Atlantic region. Our set up of the MetUM uses the Global Atmosphere 6 and Global Land 6 (GA6/GL6) configurations including the ENDGame dynamical core (Walters et al. 2017). One modification to the standard GA6/GL6 configuration was to include form drag in the surface momentum exchange over sea ice, based on Lüpkes et al. (2012) and Elvidge et al. (2016), and now part of the GL8 configuration. This new scheme has recently been implemented in the operational forecasting suite following evidence of significant improvements in simulated fluxes of momentum and heat and consequently improvements to the representation of wind speeds and temperatures over-and-downwind of the marginal-ice-zone during Arctic CAOs (Renfrew et al. 2019a). In our set up the MetUM was run globally with an N320 longitude-latitude grid (0.56° x 0.375°, equivalent to 60 km by 42 km at the equator) and 70 vertical levels up to a height of 40 km. With an Iceland and Greenland Seas nested domain of 200 x 210 grid points using a grid spacing of 0.072° x 0.072° (equivalent to 8 km by 8 km) centred on 70.8°N, 14.0°W. This horizontal resolution is sufficient to capture mesoscale weather systems, such as polar mesoscale cyclones and barrier flows, that contribute to elevated surface fluxes and represent sea-ice distributions with fidelity. The nested domain is shown in Figure 1 (and subsequent figures).

The MetUM was run in atmosphere-only mode with SST and sea-ice fields prescribed at the lower boundary for both the global and regional nested domains. The SST and sea-ice data were taken from the Operational Sea Surface Temperature and Sea Ice Analysis (OSTIA) system (Donlon et al. 2012; Roberts-Jones et al. 2012) and re-gridded to match the respective resolutions of the global model and the nested domain. The lower boundary conditions were updated daily. Within our set up, the global model was re-initialised daily at 00 UTC by ERA-Interim reanalysis (Dee et al. 2011). After initialisation on the first day of the simulation, the nested domain was only forced at the lateral boundaries by the global model. This means the nested domain was able to spin up and maintain mesoscale structures, within a regional atmospheric circulation environment that is nudged towards reality on a daily basis. The nested domain was relatively small, so strongly influenced by the lateral boundary conditions. All simulations were run across an extended winter period, 1^{st} November to 30^{th} April, for 20 seasons from winter 1990/91 to 2009/10.

2.2. Experimental Design

We produced three simulations each with a different *annually-repeating daily SST and sea-ice* lower boundary condition:

- Ice$_{max}$ simulation – Lower boundary conditions taken from the winter with the largest winter-mean sea-ice extent, namely 1987/88.
- Ice$_{med}$ simulation - Lower boundary conditions taken from the winter with the median winter-mean sea-ice extent, namely 2003/04.
- Ice$_{min}$ simulation - Lower boundary conditions taken from the winter with the smallest winter-mean sea-ice extent, namely 2015/16.

The largest, median and smallest winter sea-ice extents were determined for the Iceland and Greenland Seas region by comparing annual January-April anomalies from the OSTIA dataset to the

1979-2016 mean. Note a 'baseline' simulation with annually-varying daily SST and sea ice was also run and checked for fidelity with respect to ERA-Interim reanalyses. It corresponded very well on synoptic-scales, giving confidence that in our experiments we are effectively down-scaling the 'real' atmosphere but with different surface conditions. The baseline simulation is not analysed any further here.

3. Results

3.1. Climatological response to anomalous surface boundary conditions

Figure 1 displays monthly mean sea-ice concentration for the Ice_{med} simulation and sea-ice concentration anomalies (relative to Ice_{med}) for the Ice_{max} and Ice_{min} simulations. In the Ice_{max} simulation large sea-ice anomalies exist in all months and especially in January and April. The Ice_{max} simulation emphasises the Odden Ice Tongue, a feature that was intermittently present in the Greenland Sea during the 1980s and 1990s and has been previously linked to open ocean convection in the region (Waddams 1998; Waddams & Comiso 1999). In the Ice_{min} simulation, the largest anomalies occur in February and March, distributed along the whole ice edge. In January and April, there is a north-south split: with less sea ice in the south and more sea ice in the north.

The corresponding SST anomalies are given in Figure 2. These show broadly lower SSTs during the Ice_{max} simulation and broadly higher SSTs during the Ice_{min} simulation (compared to the Ice_{med} simulation) especially over the Greenland Sea. Anomalies in the simulated air temperature at 1.5 m (T_a) are largely coincident with the sea-ice concentration anomalies, i.e. when sea ice is anomalously present there is a cold anomaly; when it is anomalously absent there is a warm anomaly (compare Fig. 3 with Fig. 1). Away from the ice edge and over the open ocean, T_a anomalies are strongly related to anomalies in SST (compare Fig. 3 with Fig. 2) and are restricted in magnitude to <2 K. Note statistical significance using the Mann-Whitney-Wilcox test has been examined for T_a and other variables and most of the region of interest has statistically significant differences at the 95% confidence level (not shown).

There are also large differences in the monthly mean surface heat fluxes (SHF - the sum of the surface sensible and surface latent heat fluxes) in the three simulations (Fig. 4). Examining Ice_{max} - Ice_{med} there is a general reduction in heat fluxes that is most pronounced over large areas of anomalously present sea ice (differences of -125 W m^{-2}). In January, the large negative anomaly over the Odden Ice Tongue is accompanied by a positive anomaly to the south, between the sea ice and

Iceland, where cold air outbreak surface fluxes will be at their largest in the Ice_{max} simulation. Note, that we use the convention that a positive heat flux represents a transfer of energy from the ocean into the atmosphere. In the Ice_{min} - Ice_{med} results there is a pronounced strip of anomalously high SHF associated with the reduced sea-ice cover. This strip is most pronounced in February and March (differences of over 125 W m^{-2}). It is weaker and confined to the south in January and is more diffuse in April.

Figures 3 and 4 show a strong mean lower-atmospheric response to sea-ice cover, especially in the Iceland Sea. With a view to understanding how changes in the marginal ice zone impact on oceanic convection, here we will focus on two gyres, the Iceland Sea gyre (between Iceland and Jan Mayen) and the Greenland Sea gyre (between Jan Mayen and Svalbard); the same gyres investigated by Moore et al. (2015). We have defined boxes over each gyre and calculate spatial averages of surface heat flux over each box.

Averaging over the Iceland Sea gyre there is a *decrease* of 15% in seasonal (JFMA) average surface heat flux between the Ice_{max} and Ice_{min} simulations (Table 1). There is, however variation in heat flux differences across the winter months. For the Ice_{max} simulation the strongest anomalies in T_a and surface heat flux are in January (Figs. 3b, 4b), with more modest anomalies in February-April. This is reflected in the monthly heat flux averages for the Iceland Sea gyre, which show a 30% decrease in January, compared to decreases of 10%, 6% and 5% in February, March and April (Table 1). The mean lower-atmospheric response to sea-ice cover in the Greenland Sea is generally weaker (Figs. 3, 4). In fact, when averaged over the Greenland Sea gyre there is a surprising *increase* of 8% in seasonal average heat fluxes between the Ice_{max} and Ice_{min} simulations and similar increases for each month (Table 1). The reasons for this increase are discussed below.

In summary, the Ice_{max}, Ice_{med}, and Ice_{min} simulations produce anomalous responses in near-surface air temperatures of up to several degrees and in surface heat fluxes of up to $\pm$125 W m^{-2} (comparable to the domain mean), despite having identical large-scale atmospheric forcing. It is clear from these simulations that sea-ice cover profoundly affects the surface fluxes in this region.

3.2. High heat flux events and their response to anomalous surface boundary conditions

The consistent large-scale atmospheric circulation across our experiments makes it possible to carry out a comparison of high heat flux events that are common to all three simulations over the 20 winter seasons. For our two gyres, *high heat flux events* are identified individually for each gyre as periods when the surface heat fluxes exceed a threshold value, here set as 50 W m^{-2}. Our results are not qualitatively sensitive to this value. For this threshold there are 177 (199) high heat flux events during JFMA in the Iceland (Greenland) Sea gyre that are common to all three simulations. Note, that when consecutive days exceed the threshold, the peak magnitude is selected as representing the event. An analysis comparing the average magnitude (all days exceeding the threshold in the event) to the peak magnitude as a method to identify events that displayed no significant differences.

In an event-by-event comparison for the Iceland Sea gyre, the majority (76%) of high heat flux events had higher fluxes in the Ice_{max} simulation than in the Ice_{min} simulation (Table 2). In January 96% of events in Ice_{max} have higher heat fluxes; while in April 55% of events have higher heat fluxes. The impact of sea-ice cover on the magnitude of high heat flux events weakens dramatically during the winter. This is consistent with the mean SHF differences which are 44 W m^{-2} in January and 5 W m^{-2} in April (Table 1).

In an event-by-event comparison for the Greenland Sea gyre, the opposite was true. The high heat flux events had higher magnitude in the Ice_{min} simulations. Averaged over JFMA 93% of events in Ice_{min} have higher heat fluxes with this fraction of events consistent over the winter (Table 2). This is consistent with the mean SHF differences which are confined to a range of 9-14 W m^{-2} (Table 1). In the Greenland Sea gyre changes in the sea ice over the winter have less effect on the SHF. At first this finding may seem counterintuitive, but an examination of the sea-ice concentration fields (Fig. 1) shows that to the west of the Greenland Sea gyre the ice edge is relatively unchanged in January, changes by only a moderate amount in February and March, and is actually further east in April. This suggests that sea-ice differences are probably not responsible for the heat flux differences seen in the experiments. Examining Fig. 2 it is clear there is a widespread difference in the SSTs in the experiments. In the Ice_{min} simulation the SST is 1-2 K higher than in the Ice_{med} simulation in the vicinity of the Greenland Sea gyre in all four months; while in the Ice_{max} simulation the SST is 1-2 K lower than in the Ice_{med} simulation. It would appear that this difference in SST dominates over the differences in air temperatures and is responsible for the higher heat fluxes during reduced sea-ice conditions in the Greenland Sea gyre.

3.3 Isolating the role of anomalous sea ice from the compensating effects of co-varying SST anomalies

There are two factors determining the surface heat fluxes in our simulations: the prescribed SSTs, which are different in the three experiments (Fig.2); and the near-surface air temperatures and wind speeds, which are determined by the model and primarily driven by changes in the sea ice (Fig.1). Results in the previous two sub-sections reveal that in years with more extensive sea ice the adjacent open-ocean SSTs are generally anomalously low; while in years with less extensive sea ice, SSTs are generally anomalously high (Figs. 1, 2). This means that with reference to a fixed location, such as the two gyres, the relative difference, $\Delta T = (SST - T_a)$, is what determines the magnitude of surface heat fluxes. During a CAO over more (less) extensive sea ice then both the atmosphere and ocean will be colder (warmer), and physical reasoning suggests that ΔT could be either higher or lower as a result. In other words, the role of the sea ice distribution in determining surface heat fluxes is contingent on the SST distribution prescribed.

In this section we isolate the impact of anomalous sea ice distributions on heat flux events by estimating and removing the compensating effects of co-varying anomalous SST patterns. The approach taken is to re-calculate the surface heat fluxes 'offline' using a simple bulk flux formula (e.g. Gill 1982). We re-calculate the sensible heat flux (Q) for two scenarios: (i) a control scenario that emulates the simulations and has SSTs and sea ice from the same model runs; and (ii) an alternative scenario that has bulk formula input switched, i.e. SST from Ice_{max} (SST_{max}) is used along with atmospheric output from Ice_{min}. For the matching SSTs, (when Q was calculated using input from the same simulation) there are two versions, '$Q_{SSTmax\_Ta\_max}$' and '$Q_{SSTmin\_Ta\_min}$':

$$Q_{SSTmax\_Ta\_max} = \rho_a C_p C_H U_{max} (SST_{max} - T_{a\_max}), \qquad \text{Eq. 1a.}$$

$$Q_{SSTmin\_Ta\_min} = \rho_a C_p C_H U_{min} (SST_{min} - T_{a\_min}). \qquad \text{Eq. 1b.}$$

For the switched SSTs, there are again two calculations of sensible heat flux, '$Q_{SSTmin\_Ta\_max}$' and '$Q_{SSTmax\_Ta\_min}$':

$$Q_{SSTmin\_Ta\_max} = \rho_a C_p C_H U_{max} (SST_{\_min} - T_{a\_max}) , \qquad \text{Eq. 2a.}$$

$$Q_{SSTmax\_Ta\_min} = \rho_a C_p C_H U_{min} (SST_{\_max} - T_{a\_min}) , \qquad \text{Eq. 2b.}$$

where, T_a is air temperature at 1.5 m, SST is sea surface temperature, U is 10 m wind speed , C_p is the heat capacity of air (1004 J kg^{-1}), ρ_a is the air density at the surface (set here to 1.225 kg m^{-3}), and C_H is the non-dimensional Stanton number (set here to be 0.0011). The value for the Stanton number was obtained from Smith (1980), and this value has been shown to match well to observations (i.e. Cook & Renfrew, 2015). In all cases, the subscripts 'max' and 'min' refer to the

Ice_{max} and Ice_{min} simulations for SST, T_a and U. . Note the above uses a simplified bulk flux algorithm compared to what is used in the MetUM, which has a stability-dependent C_H and varying ρ_a. However, validation of the offline fluxes against model output did not raise any concerns, so we argue they are appropriate for the sensitivity testing undertaken here. For these sensitivity tests, the bulk fluxes are calculated as a composite based on all the high heat flux events in each gyre (177 in the Iceland Sea gyre and 199 in the Greenland Sea gyre).

(i) The SST effect

For both the Iceland Sea and Greenland Sea gyres, the magnitude of the bulk-flux-estimated value for Q increases when the SST input is switched from SST_{max} (anomalous cold) to SST_{min} (anomalously) warm in the Ice_{max} bulk flux calculations (Fig. 5). There is an increase of 29 W m^{-2} (11%) in the Iceland Sea gyre and 46 W m^{-2} (15%) in the Greenland Sea gyre. As might be expected there are corresponding decreases when the SST input is switched from SST_{min} to SST_{max} in the Ice_{min} case bulk flux calculations (Fig. 5b). The Iceland Sea gyre fluxes decrease by 37 W m^{-2} (-17%) and the Greenland Seas gyre fluxes decrease by 49 W m^{-2} (-15%). These anomalies represent the effect of changing the SST forcing, with only the SST term altered in the bulk flux calculations.

ii) The isolated sea-ice effect

Using the offline bulk flux re-calculations we can isolate the effects of retreating sea ice on surface fluxes; specifically, $Q_{SSTmax\_Ta\_min}$ can be compared with $Q_{SSTmax\_Ta\_max}$ (SST_{max} case) and $Q_{SSTmin\_Ta\_min}$ with $Q_{SSTmin\_Ta\_max}$ (SST_{min} case). We found that a reduction in sea-ice extent consistently leads to a decrease in the magnitude of high heat flux events for both gyres (Fig. 6). For the Iceland Sea gyre, the change is -72 W m^{-2} (-40%) for the SST_{max} case and -64 W m^{-2} (-29%) for the SST_{min} case. For the Greenland Sea gyre, the change is -24 W m^{-2} (-8%) for the SST_{max} case and -21 W m^{-2} (-6%) for the SST_{min} case. With each gyre, there are only slight differences between calculations with anomalously warm and cold SSTs, suggesting that the differences in wind speed are insignificant with respect to their impact on the bulk flux calculations. These offline sensitivity tests employ a simplified formula for surface sensible heat flux that allows easy substitution of variables. It is expected that the surface latent heat flux sensitivities would be similar as the surface turbulent heat fluxes are strongly correlated during CAO (e.g. Papritz and Spengler 2017).

In summary, the above results show that over the Iceland Sea, variability and trends in sea-ice extent have a significant impact on high heat flux events (more than 60 W m^{-2} in magnitude) that is only partially offset by co-varying SSTs. Over the Greenland Sea, the smaller variations in sea-ice extent combined with larger amplitude co-variability in SSTs mean that the sea-ice extent effect is small (around 20 W m^{-2} in magnitude) and it is SST differences (around 45 W m^{-2} in magnitude) that dominates the overall impact on high heat flux events. Our results imply that sea-ice retreat may affect the Iceland Sea region more profoundly than the Greenland Sea region.

3.4 Case study and composite analysis of the relationship between SST and sea ice on heat fluxes

To illustrate why the relationship between the lower boundary conditions and surface heat fluxes is so different between the Iceland Sea and Greenland Sea gyres, we present two case studies. Figure 7 shows a case for the Iceland Sea gyre, when the heat fluxes are greater in the Ice_{max} simulation than the Ice_{min} simulation. The case is from 31st January 1995, when a pressure gradient between Greenland and the Iceland Sea results in northerly wind flow over the Iceland Sea gyre (Fig. 7a), bringing cold air and surface heat fluxes of up to 500 W m^{-2} focussed off the ice edge. Relative to the Ice_{med} simulation, the Ice_{max} simulation exhibits a strong positive mean sea level pressure (MSLP) anomaly (6-7 hPa - Fig. 7b) and a negative air temperature anomaly (5-7 K – Fig. 7e) which extends from over sea ice to the whole of the Iceland Sea. The Ice_{max} sea-ice cover leads to large differences in heat fluxes strongly reduced over the sea ice and strongly increased over the Iceland Sea gyre, by more than 200 W m^{-2} (Fig. 7h). The impact of the maximum versus median sea-ice distributions on heat fluxes in this case is significant. In the Ice_{min} simulation, the reduced sea-ice extent provides a large fetch of ice-free ocean to the north of the Iceland Sea Gyre which results in a positive air temperature anomaly (about 3 K - Fig 9f) in the Ice_{min} simulation and a small -20 W m^{-2} negative heat flux anomaly in the Iceland Sea. In the Ice_{min} - Ice_{med} comparison, the positive heat flux anomalies are limited to the sea-ice edge, consistent with the monthly anomalies for the Ice_{min} simulation (Fig. 4).

Figure 8 illustrates a case for the Greenland Sea gyre when heat fluxes are greater in the Ice_{min} simulation than in the Ice_{max} simulation. On the 25th February 1993 a high pressure system over Greenland extending south over Iceland combined with low pressure to the East and NE results in westerly flow over the location of the Greenland Sea gyre (Fig. 8a). Associated with this a cold air mass covers Greenland and the NW Greenland Sea, leading to surface heat fluxes of up to 400 W m^{-2}, with maxima off the sea-ice edge. The westerly flow in this region results in the air flow into the Greenland Sea gyre passing over a region with small differences in the sea-ice extent between the Ice_{max}, Ice_{med} and Ice_{min} simulations. In the vicinity of the Greenland Sea gyre, the Ice_{max} simulation displays small anomalies in MSLP (< 0.5 hPa; Fig. 8b) and T_a (~0.5 K; Fig. 8e), and a modest negative heat flux anomaly between -75 and -50 W m^{-2} (Fig. 8h). The Ice_{min} simulation displays notable negative MSLP (2 hPa; Fig. 8c) and positive T_a (1-2 K; Fig. 8f) anomalies, and a corresponding positive heat flux anomaly of 75 to 100 W m^{-2} (Fig. 8i). Consequently the difference between the Ice_{min} and Ice_{max} simulations for this case is a combination of these moderate heat flux anomalies that is primarily driven by SST differences (not shown) rather than the moderate air temperature differences (Figs. 8e,f).

For each gyre, the case studies highlight the physical mechanism by which the high heat flux events occur, with northerly flow driving marine CAOs in the Iceland Sea gyre and westerly flow driving CAOs in the Greenland Sea gyre. For these case studies, the different circulation patterns are consistent with the hypothesis regarding the role of SSTs in compensating for the sea-ice distribution differences.

To assess the generality of this result, a composite analysis of all high heat flux events was undertaken. Figure 9 shows the composite MSLP for high heat flux events over the Iceland Sea gyre, the Greenland Sea gyre and for all simulated days. Figure 9a shows that for the Iceland Sea gyre pressure is higher over continental Greenland with lower pressure over the open ocean to the east of the domain. This is associated with a northerly wind across the region, which, as shown in the case study, results in CAO events that drive high heat fluxes in the Iceland Sea. There are qualitative similarities between the composite Iceland Sea gyre circulation pattern (Fig. 9a), the Iceland Sea gyre case study (Fig. 7a) and a composite of ERA Interim data for buoy-observed high heat flux events shown in Harden et al. (2015).

For the Greenland Sea gyre (Fig. 9b), the composite shows a maximum in MSLP over coastal Greenland and adjacent sea-ice regions. While the composite flow is more north-westerly than the westerly flow seen in the case study (Fig. 8a), it still represents a similar trajectory of air flow over the Greenland Sea gyre, and its interaction with a region of only small differences in sea ice between the three simulations (Fig. 1). In each case the circulation pattern is significantly different to that in the simulated extended winter mean climatology (Fig. 9c), which exhibits much smaller pressure gradients, and corresponding weaker winds. The mean climatological MSLP and wind distribution (Fig. 9c) is consistent with the Iceland Sea being a saddle point in North Atlantic MSLP and a regional heat flux minimum (e.g. Moore et al. 2012; Harden et al. 2015; Papritz & Spengler 2017).

Via the case studies and the composite analyses, it is evident that a difference in response exists between the Iceland Sea and Greenland Sea gyres. For the Iceland Sea gyre, strong northerly flow interacts with the highly variable sea ice of the northern Iceland Sea, leading to dramatic differences in heat fluxes. Here the sea ice distribution is the primary factor in the distribution and magnitude of surface heat fluxes in the different simulations. Differences in the SST are secondary.

For the Greenland Sea gyre, high heat flux events occur during westerly or north-westerly flow, resulting in the air mass interacting with a region where sea ice is much less variable. Consequently, the different sea-ice distributions in our simulations do *not* primarily control the surface heat fluxes here. Instead, the SST differences dominate and the heat flux magnitude is higher in the Ice_{min} simulation rather than the Ice_{max} simulation. In offline recalculations when this SST effect is controlled for (Figs. 5,6), the Ice_{max} simulation displays stronger magnitude heat fluxes than the Ice_{min} simulation, consistent with responses for the Iceland Sea gyre where anomalous sea ice dominates over the SST effect.

4. Discussion and Conclusions

We have run three regional climate simulations using the MetUM at 8 km grid size with different annually repeating surface sea ice and SST fields taken, from the years with the largest, median and smallest sea-ice extent from the satellite era for this region. These experiments have facilitated comprehensive assessment of the impacts of anomalous sea-ice conditions (and corresponding sea surface temperatures) on the gyres within the Iceland Sea and the Greenland Sea.

The surface heat fluxes in these gyres are significantly affected by changes in the adjacent sea-ice distributions and SSTs. For the Iceland Sea gyre, differences due to the sea-ice distribution dominate, with differences due to the SST of secondary importance. Composite and case study analysis highlights that high heat flux events in the Iceland Sea occur during northerly flow and pass over a region of large sea-ice variability. The impact of this variability on downstream surface heat fluxes can be large (>100 W m^{-2}); in keeping with idealised modelling experiments (e.g. Liu et al. 2006; Chechin et al. 2013). Composite analysis of high heat flux events is consistent with previous composites and buoy observations (see Harden et al. 2015). Our results provide evidence for the hypothesis of Moore et al. (2015) that a retreating wintertime sea-ice extent is contributing to a reduction in the surface heat fluxes over the Iceland Sea.

For the Greenland Sea gyre, differences in heat fluxes due to the sea-ice distribution are surprisingly small and differences due to the SST dominate. Composite and case study analysis of high heat flux events show these occur during predominantly westerly or north-westerly winds, and so pass over a region of relatively little sea-ice variability. The SST associated with maximum (minimum) sea-ice extents is anomalous low (high), as would be expected. The impact of this on ΔT dominates the surface heat flux differences in our experiments. However we have also shown that when the SST change is controlled for, the change in sea-ice distribution does impact the surface fluxes as expected, i.e. in the same manner as the Iceland Sea region.

Our results for the Greenland Sea gyre do *not* support one of the hypotheses of Moore et al. (2015) that a retreating wintertime sea-ice extent is contributing to a reduction in the surface heat fluxes over the Greenland Sea. Moore et al. show a decrease in heat fluxes that begins in the mid-1990s and coincides with a decrease in sea ice in the Greenland Sea. They suggest that the decrease in heat flux is due to the sea-ice retreat *and* differential warming of the atmosphere and ocean. By design, we have not examined this second mechanism explicitly. But we have shown that for the Greenland Sea region, the SST effect dominates the differences between the experiments and this implies that the differential warming mechanism is more important in this location. It is worth noting that Moore et al. (2015) present results for winter mean heat fluxes (c.f. our Table 1), while the latter part of our analysis focuses on high heat flux events (Table 2; Figs. 7, 8).

Given the importance of deep-water formation in the Greenland Sea gyre for both the formation of dense water in the Iceland Sea (Moore et al. 2015) and the North Icelandic Jet (Våge et al. 2011), it is important to determine the importance of both the short timescale high heat flux events and the long timescale conditioning of the winter time Greenland Sea ocean and heat fluxes. In both gyre regions, the relationship between changes in sea ice and SSTs lead to generally compensating impacts on high heat flux events, whereby decreased sea ice acts to reduce their magnitude, whilst the associated higher SST acts to enhance heat fluxes.

The novel experimental design used here has allowed a quantification of the role of changes in both sea-ice distribution and SSTs on the magnitude of high heat flux events in the Iceland Sea and Greenland Sea gyres. Based on our results, we conclude that variability in sea-ice dominates the variability of heat fluxes in the Iceland Sea gyre; whilst variability in SST dominates variability of heat fluxes in the Greenland Sea gyre. However, these high heat flux eventsare predominantly generally cold air outbreaks, so are a result of the large-scale atmospheric circulation and occur whatever the surface conditions. Consequently, it will be important to understand the interaction between changes in sea ice and SSTs and large-scale patterns of variability such as the North Atlantic Oscillation and the East Atlantic Pattern; including how these circulation patterns are changing under anthropogenic forcing. The experimental design here focused on isolating the impacts of sea-ice distribution and SST on surface heat fluxes and so used an atmosphere-only model with prescribed surface conditions. In reality, the climate system is tightly coupled in these subpolar seas and feedbacks between the atmosphere and ocean during sea-ice change are likely to play a role. This aspect should be examined in a coupled framework in a future study.

Acknowledgements

JOP, TJB, IAR and ADE acknowledge the support of the Natural Environment Research Council (NERC) grant: NE/N009924/1 and NE/N009754/1 (Atmospheric Forcing of the Iceland Sea – the UK's contribution to the Iceland Greenland Seas Project). We are grateful to the ECMWF for the provision of the ERA-Interim meteorological fields (available here: http://apps.ecmwf.int/datasets/data/interim-mdfa/). The OSTIA data was downloaded from the Copernicus Marine Environment Monitoring Service. It is identified in their system as: SST_GLO_SST_L4_REP_OBSERVATIONS_010_011 and access to the data can be found here: http://marine.copernicus.eu/services-portfolio/access-to-products/?option=com_csw&view=details&product_id=SST_GLO_SST_L4_REP_OBSERVATIONS_010_011. Model data fields used in this study will be available from the IGP Project archive at the Centre for Environmental Data Analysis, which can be found here: https://catalogue.ceda.ac.uk/uuid/2780d047461c42f0a12534ccf42f487a. The code for the heat flux event algorithm can be accessed via the IGP GitHub repository here: https://github.com/IGPResearch/bas. The authors would like to thank Dr Stuart Webster (UK Met Office) for his assistance in setting up and using the MetUM Nested Suite and Willie McGinty (National Centre for Atmospheric Science) for assistance in producing model GRIB files from the ERA-Interim reanalysis. Simulations were run on the UK Met Office HPC facility MONSooN from February 2018 to September 2018. We would like to thank the two anonymous reviewers for their comments which improved the final manuscript and the accessibility of the figures.

References

Arzel O, Fichefet T, Goose H (2006) Sea ice evolution over the 20th and 21st centuries as simulated by current AOGCMs. Ocean Model 12:401-415.

Brümmer B (1997) Boundary layer mass, water and heat budgets in wintertime cold-air outbreaks from the Arctic sea ice. Mon Wea Rev 125:1824–1837.

Cavalieri DJ, Parkinson CL (2012) Arctic sea ice variability and trends, 1979–2010. Cryosphere 6 881-889 https://doi.org/10.5194/tc-6-881-2012

Chechin DG, Lüpkes C, Repina IA, Gryanik VM, (2013) Idealized dry quasi 2-D mesoscale simulations of cold-air outbreaks over the marginal sea ice zone with fine and coarse resolution. J Geophys Res Atmos 118(16) 8787-8813 https://doi.org/10.1002/jgrd.50679

Chechin DG, Lüpkes C, (2017) Boundary-layer development and low-level baroclinicity during high-latitude cold-air outbreaks: a simple model. Boundary-Layer Meteorol 162: 91. https://doi.org/10.1007/s10546-016-0193-2

Condron A, Bigg GR, Renfrew IA, (2008) Modelling the impact of polar mesoscale cyclones on ocean circulation. J Geophysical Res (Oceans) 113 C10005, doi:10.1029/2007JC004599.

Condron A, Renfrew IA, (2013) The impact of polar mesoscale storms on northeast Atlantic Ocean circulation. Nature Geoscience 6 34-37. doi:10.1038/ngeo1661

Cook PA. Renfrew IA. (2015) Aircraft-based observations of air–sea turbulent fluxes around the British Isles. Q J Roy Meteor Soc. 141 139–152 doi:10.1002/qj.2345

Dee D et al. (2011) The ERA-Interim reanalysis: Configuration and performance of the data assimilation system. Q J R Meteorol Soc 137:553–597. https://doi.org/10.1002/qj.828

Donlon CJ, Martin M, Stark J, Roberts-Jones J, Fiedler E, Wimmer W (2012) The Operational Sea Surface Temperature and Sea Ice Analysis (OSTIA) system. Rem Sens Env 116:140-158. https://doi.org/10.1016/j.rse.2010.10.017

DuVivier AK, Cassano JJ, Craig AP, Hamman J, Maslowski W, Nijssen B, Osinski R, Roberts A (2016) Winter atmospheric buoyancy forcing and oceanic response during strong wind events around southeastern Greenland in the Regional Arctic System Model (RASM) for 1990–2010. J Clim 29:975–994. https://doi.org/10.1175/JCLI-D-15-0592.1

DuVivier AK, Cassano JJ, Greco S, Emmitt GD (2017) A case study of observed and modeled barrier flow in the Denmark Strait in May 2015. Mon Wea Rev 145:2385–2404. https://doi.org/10.1175/MWR-D-16-0386.1

Elvidge AD, Renfrew IA, Weiss AI, Brooks IM, Lachlan-Cope TA, King JC (2016) Observations of surface momentum exchange over the marginal-ice-zone and recommendations for its parameterization. Atmos Chem Phys 16:1545-1563. https://doi.org/10.5194/acp-16-1545-2016

Gill, AE (1982) Atmosphere-Ocean Dynamics. Academic Press, New York

Harden BE, Renfrew IA, Petersen GN (2011) A climatology of wintertime barrier winds off southeast Greenland. J Clim 24:4701–4717. https://doi.org/10.1175/2011JCLI4113.1

Harden BE, Renfrew IA, Petersen GN (2015) Meteorological buoy observations from the central Iceland Sea. J Geophys Res Atmos 120:3199–3208. https://doi.org/10.1002/(2014)JD022584

Jung, T., Serrar, S., & Wang, Q. (2014). The oceanic response to mesoscale atmospheric forcing. Geophysical Research Letters, 41, 1255–1260. doi:10.1002/2013GL059040

Kolstad EW (2017) Higher ocean wind speeds during marine cold air outbreaks. Q J R Meteorol Soc 143:2084-2092.

Liu AQ, Moore GWK, Tsuboki K Renfrew IA (2006) The effect of the sea-ice zone on the development of boundary-layer roll clouds during cold-air outbreaks. Boundary-Layer Meteorol 118 557-581. https://doi.org/10.1007/s10546-005-6434-4

Lüpkes C, Gryanik VM, Hartmann J, Andreas EL (2012) A parametrization, based on sea ice morphology, of the neutral atmospheric drag coefficients for weather predict ion and climate models. J Geophys Res 117:D13112. https://doi.org/10.1029/2012JD017630

Marshall J, Schott F (1999) Open-ocean convection: observation, theory, and models. Rev Geophys 37:1–64. http://doi.org/10.1029/98RG02739

Michel, C., Terpstra, A., & Spengler, T. (2018). Polar mesoscale cyclone climatology for the Nordic Seas based on ERA-Interim. *Journal of Climate*, *31*(6), 2511-2532.

Mioduszewski J, Vavrus S, Wang M (2018) Diminishing Arctic Sea Ice Promotes Stronger Surface Winds. J Clim 31:8101-8119. https://doi.org/10.1175/JCLI-D-18-0109.1

Moore GWK, Renfrew IA (2005) Tip jets and barrier winds: A QuikSCAT climatology of high wind speed events around Greenland. J Clim 18:3713–3725. https://doi.org/10.1175/JCLI3455.1

Moore GWK, Renfrew IA, Pickart RS (2012) Spatial distribution of air-sea heat fluxes over the sub-polar North Atlantic Ocean. Geophys Res Lett 39:L18806. https://doi.org/10.1029/2012GL053097

Moore GWK, Våge K, Pickart RS, Renfrew IA (2015) Decreasing intensity of open-ocean convection in the Greenland and Iceland seas. Nat Clim Change 5:877–882. https://doi.org/10.1038/NCLIMATE2688

Onarheim IH, Eldevik T, Smedsrud LH, Stroeve JC (2018) Seasonal and regional manifestation of Arctic sea ice loss. J Clim 31:4917–4932. https://doi.org/10.1175/JCLI-D-17-0427.1

Papritz L, Spengler T (2017) A Lagrangian climatology of wintertime cold air outbreaks in the Irminger and Nordic Seas and their role in shaping air–sea heat fluxes. J Clim 30:2717–2737. https://doi.org/10.1175/JCLI-D-16-0605.1

Renfrew, I.A., G.W.K. Moore, J.E. Kristjánsson, H. Ólafsson, S.L. Gray, G.N. Petersen, K. Bovis, P.R.A. Brown, I. Føre, T. Haine, C. Hay, E.A. Irvine, A. Lawrence, T. Ohigashi, S. Outten, R.S. Pickart, M. Shapiro, D. Sproson, R. Swinbank, A. Woolley, S. Zhang, 2008: The Greenland Flow Distortion experiment, *Bull. Amer. Meteorol. Soc.,* **89,** 1307-1324.

Renfrew IA, Elvidge AD, Edwards J (2019a) Atmospheric sensitivity to marginal-ice-zone drag: local and global responses. Q J R Meteorol Soc145:1165-1179. https://doi.org/10.1002/qj.3486

Renfrew IA, et al. (2019b) The Iceland Greenland Seas Project. Bull Am Meteorol Soc 100:1795–1817 DOI: 10.1175/BAMS-D-18-0217.1.

Renfrew IA, Moore GWK (1999) An extreme cold air outbreak over the Labrador Sea: roll vortices and air-sea interaction. Mon Wea Rev 127:2379-2394.

Roberts-Jones J, Fiedler EK, Martin MJ (2012) Daily, Global, High-Resolution SST and Sea Ice Reanalysis for 1985-2007 Using the OSTIA System. J Clim 25:6215-6232. http://dx.doi.org/10.1175/JCLI-D-11-00648.1

Smith SD (1980) Wind Stress and heat flux over the ocean in gale force winds J Phys Oceanogr 10:709-726. 10.1175/1520-0485(1980)010<0709:WSAHFO>2.0.CO;2

Våge K, Papritz L, Håvik L, Spall M, Moore G (2018) Ocean convection linked to the recent ice edge retreat along east Greenland. Nat Comms 9:1287. https://doi.org/10.1038/s41467-018-03468-6

Våge K, Pickart RS, Spall MA, Moore GWK, Valdimarsson H, Torres DJ, Erofeeva SY, Nilsen JEO. (2013) Revised circulation scheme north of the Denmark Strait. Deep Sea Res I 79:20-39. https://doi.org/10.1016/j.dsr.201305.007

Våge K, Pickart RS, Spall MA, Valdimasson H, Jónsson S, Torres DJ, Østerhus S, Eldevik T (2011) Significant role of the North Icelandic Jet in the formation of Denmark Strait overflow water. Nat Geo 4:723–727. https://doi.org/10.1038/ngeo1234

Wadhams P (1998) The Odden ice tongue and Greenland Sea convection. Weather 54:83-84.

Wadhams P, Comiso JC (1999) Two modes of appearance of the Odden ice tongue in the Greenland Sea. Geophys Res Lett 26:2497–2500. https://doi.org/10.1029/1999GL900502

Walters, D et al. (2017) The Met Office Unified Model Global Atmosphere 6.0/6.1 and JULES Global Land 6.0/6.1 configurations. Geosci Model Dev 10:1487-1520. https://doi.org/10.5194/gmd-10-1487-2017

536

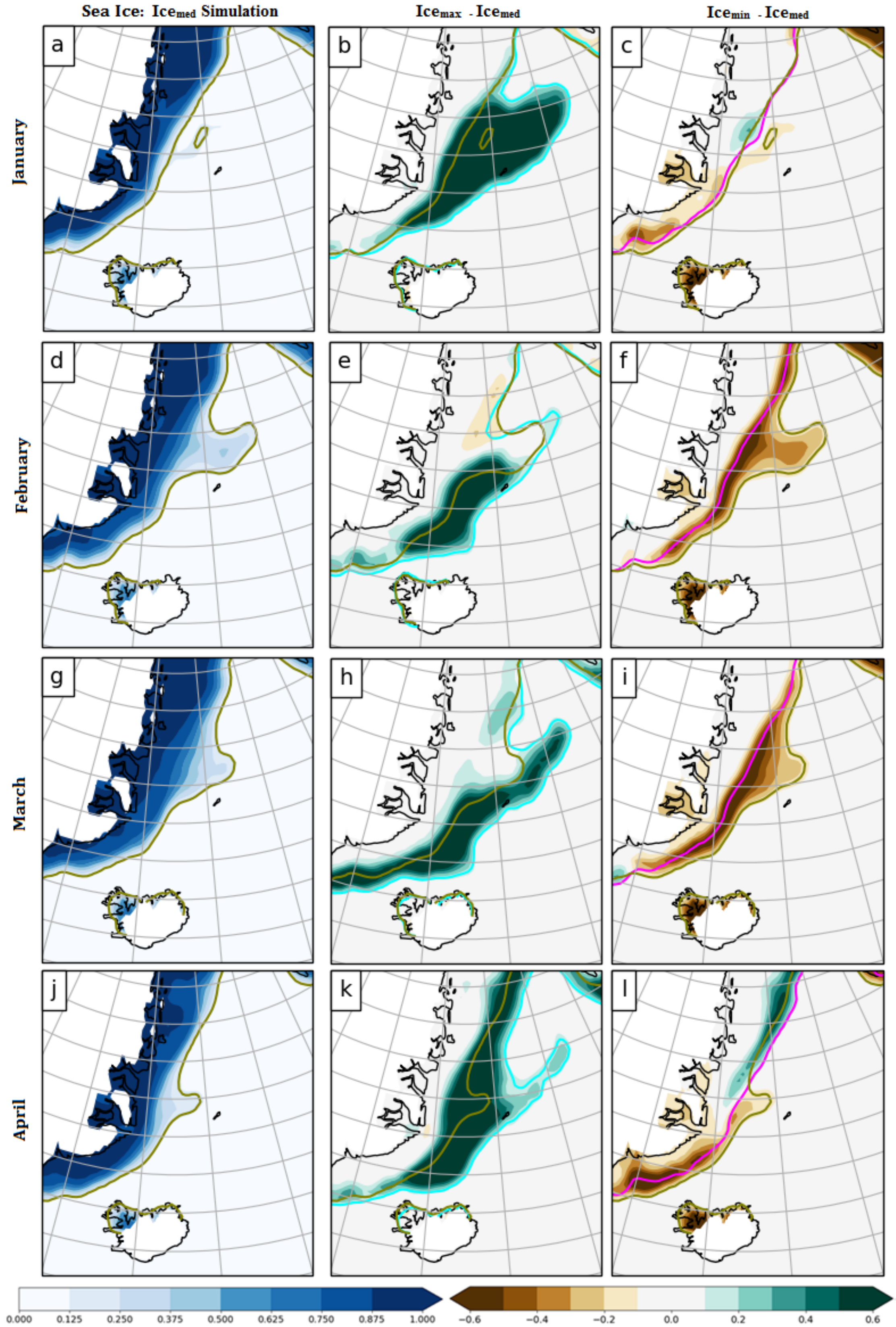

537 Figure 1 – Monthly mean sea-ice concentration for the Ice$_{med}$ simulation (a, d, g & j); and sea-ice
538 concentration anomalies for the Ice$_{max}$ - Ice$_{med}$ simulations (b, e, h & k); and the Ice$_{min}$ - Ice$_{med}$
539 simulations (c, f, i, l). The 15% sea-ice concentration contours are selectively plotted: Ice$_{max}$
540 simulation (cyan), Ice$_{med}$ simulation (olive) and Ice$_{min}$ simulation (magenta).

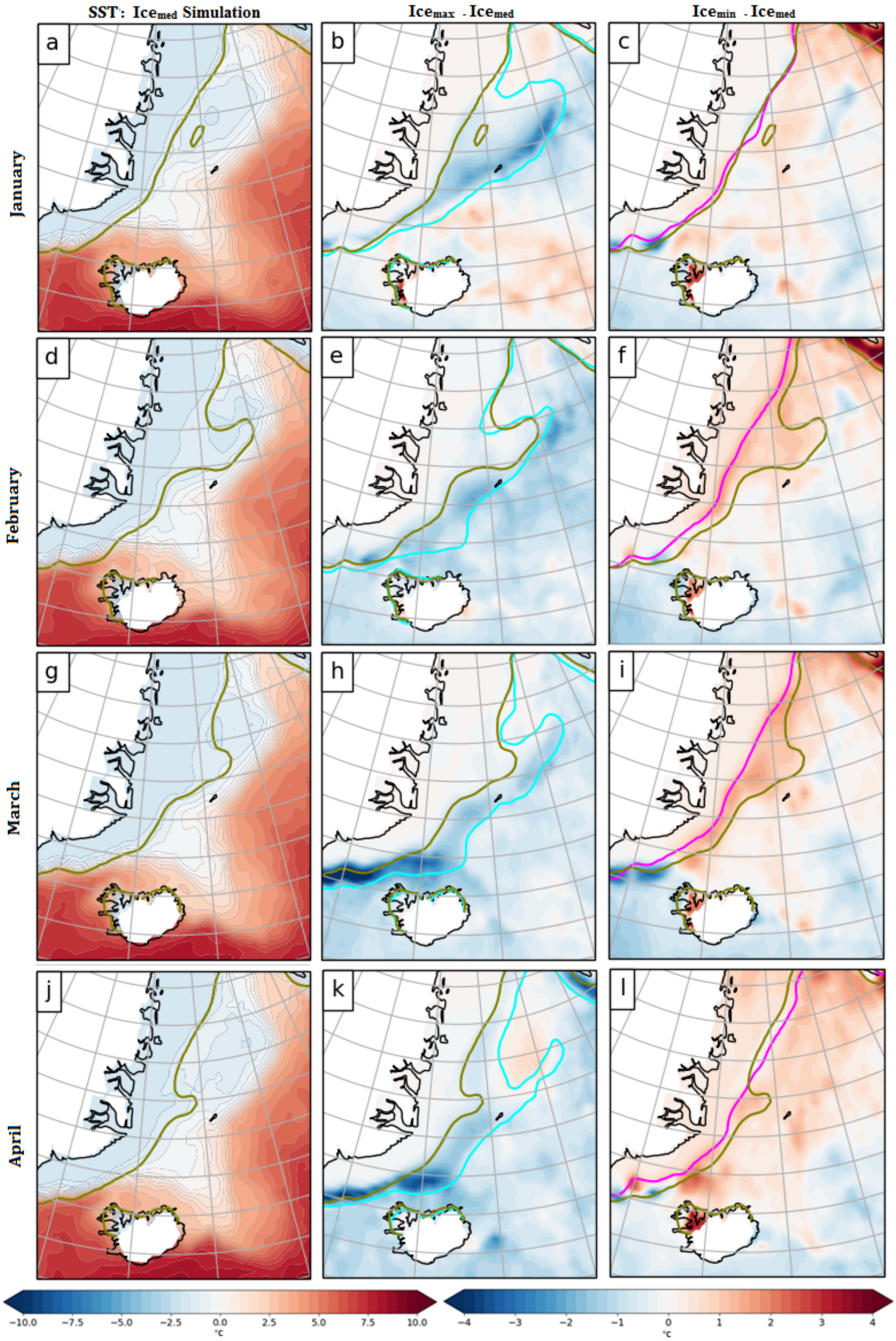

Figure 2 – Monthly mean sea surface temperature (SST, units of °C) for the Ice_{med} simulation (a, d, g & j) and SST anomalies for the Ice_{max} - Ice_{med} simulations (b, e, h & k); and the Ice_{min} - Ice_{med} simulations (c, f, i, l). The 15% sea-ice concentration contours are selectively plotted: Ice_{max} simulation (cyan), Ice_{med} simulation (olive) and Ice_{min} simulation (magenta).

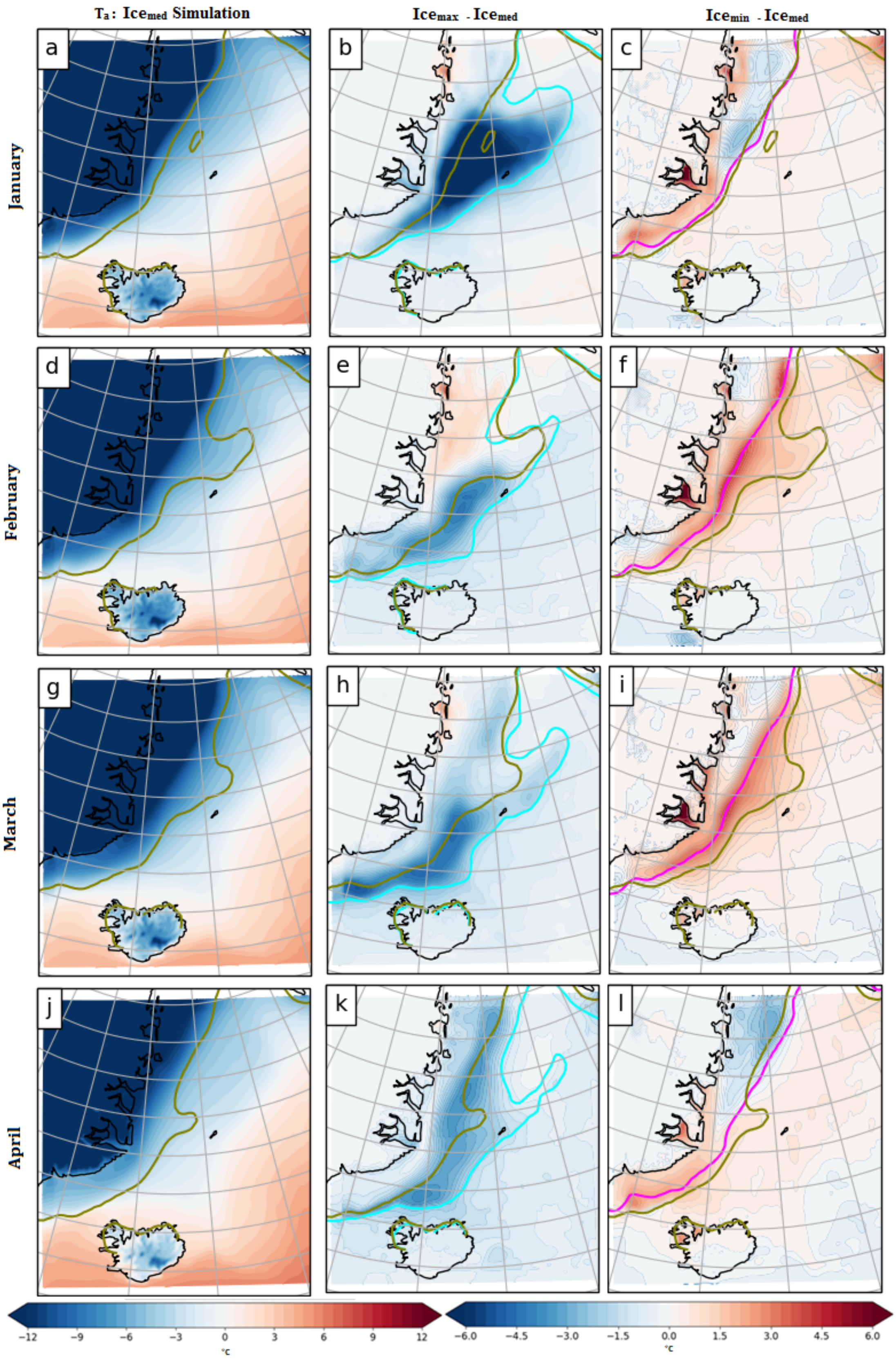

Figure 3 – Monthly mean air temperature at 1.5 m (T_a; units of °C) for the Ice_{med} simulation (a, d, g & j) and T_a anomalies for the Ice_{max} - Ice_{med} simulations (b, e, h & k); and the Ice_{min} - Ice_{med} simulations (c, f, i, l). The 15% sea-ice concentration contours are selectively plotted: Ice_{max} simulation (cyan), Ice_{med} simulation (olive) and Ice_{min} simulation (magenta).

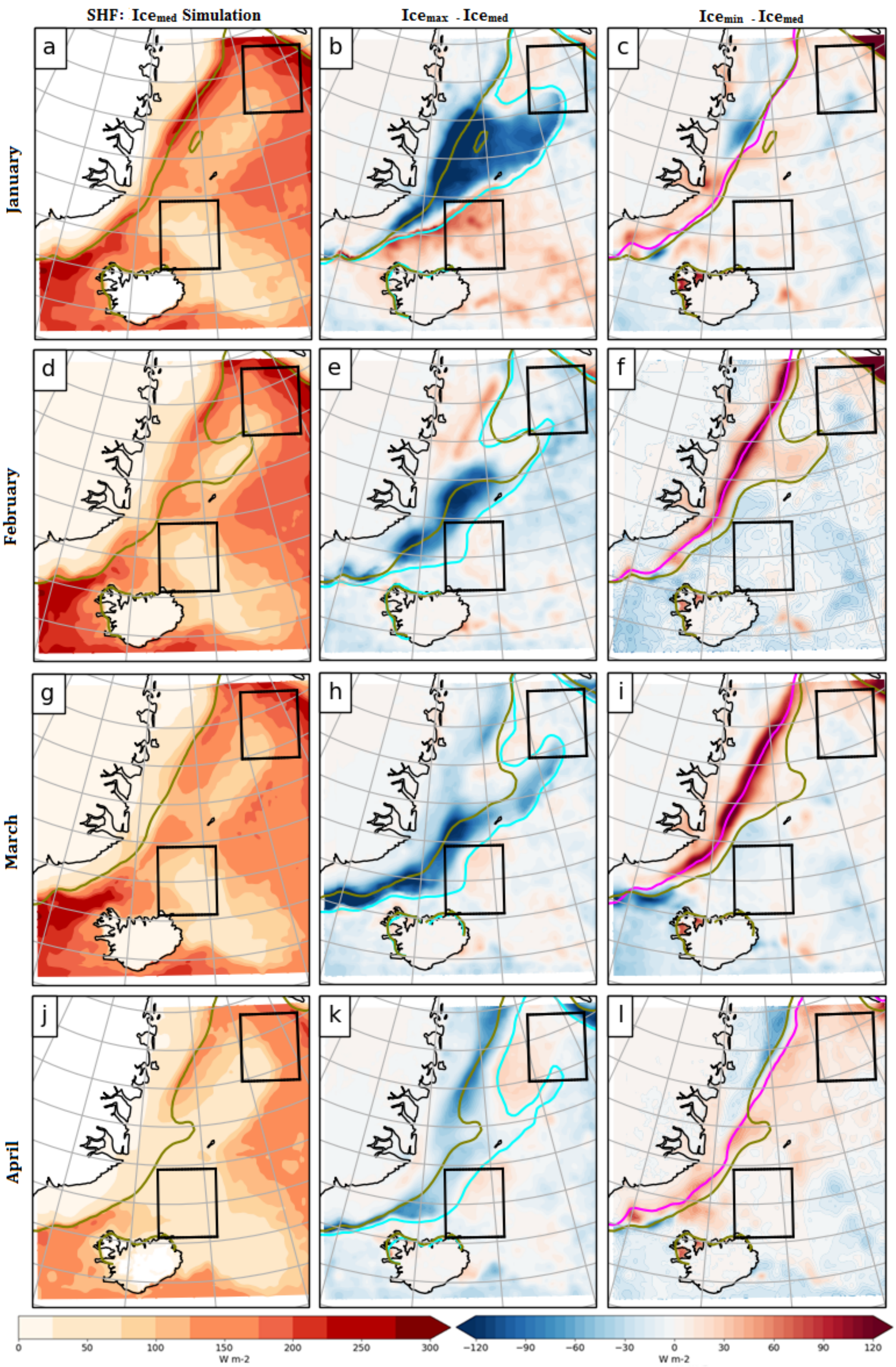

Figure 4 – Monthly mean surface heat flux (SHF; units of W m^{-2}) for the Ice_{med} simulation (a, d, g & j) and SHF anomalies for the Ice_{max} - Ice_{med} simulations (b, e, h & k); and the Ice_{min} - Ice_{med} simulations (c, f, i, l). The 15% sea-ice concentration contours are selectively plotted: Ice_{max} simulation (cyan), Ice_{med} simulation (olive) and Ice_{min} simulation (magenta). The black boxes represent the location of the Iceland Sea and Greenland Sea gyres used in this study.

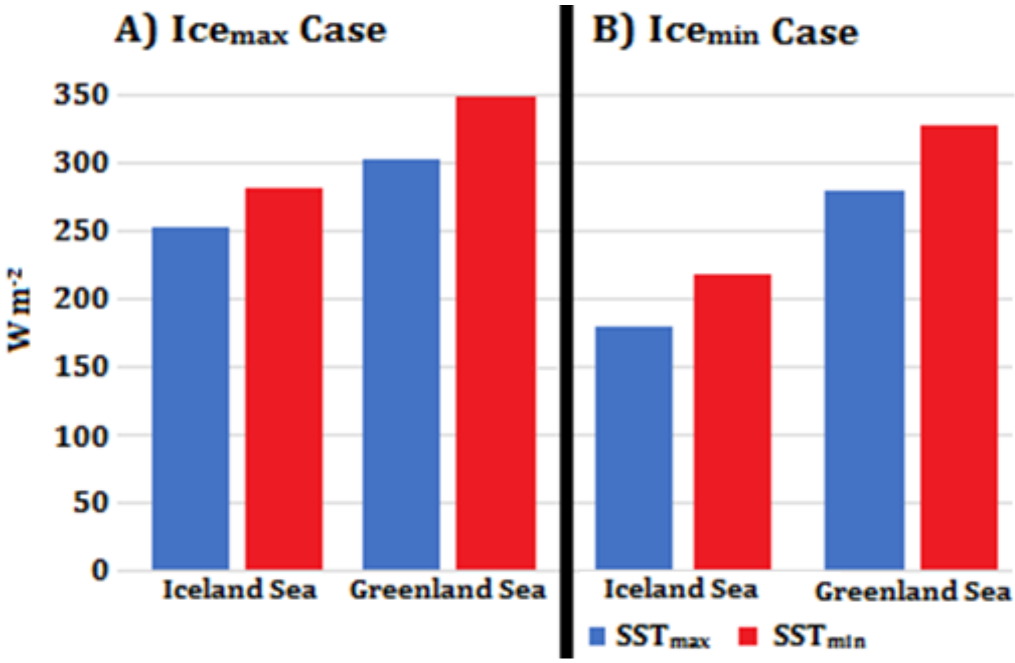

Figure 5 – Calculated sensible heat flux (Q; units of W m^{-2}) for the Iceland Sea gyre and the Greenland Sea gyre for a) the Ice$_{max}$ case ($Q_{SSTmax\_Ta\_max}$ and $Q_{SSTmin\_Ta\_max}$) and b) the Ice$_{min}$ case ($Q_{SSTmin\_Ta\_min}$ and $Q_{SSTmax\_Ta\_min}$).

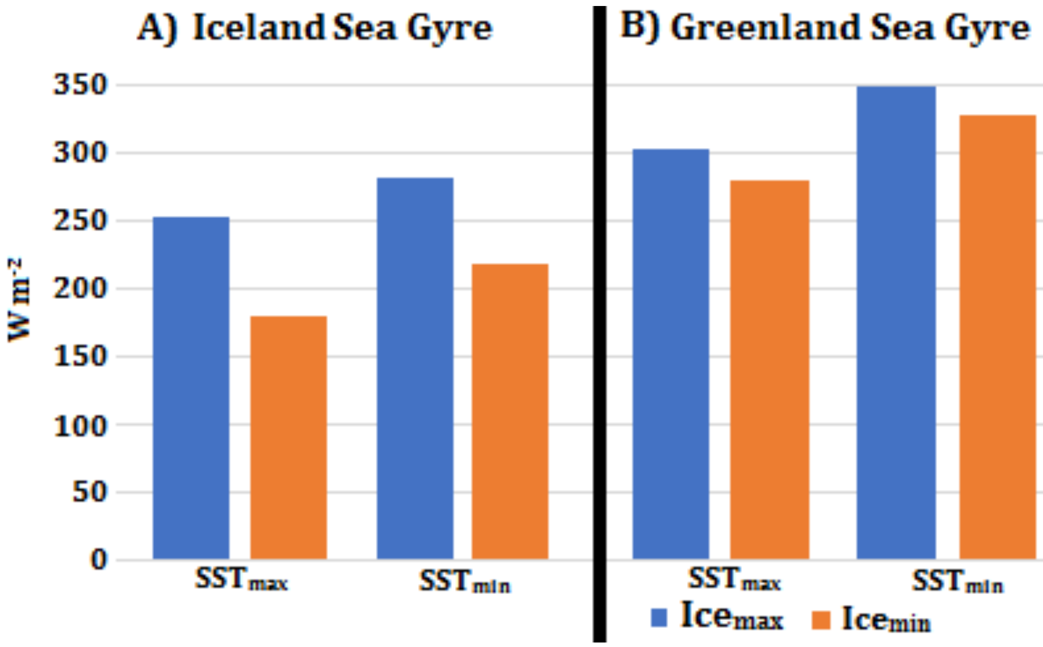

Figure 6 – Calculated sensible heat flux (Q; units of W m^{-2}) for the SST$_{max}$ case ($Q_{SSTmax\_Ta\_max}$ and $Q_{SSTmax\_Ta\_min}$) and the SST$_{min}$ case ($Q_{SSTmin\_Ta\_min}$ and $Q_{SSTmin\_Ta\_max}$) for a) the Iceland Sea gyre and b) the Greenland Sea gyre.

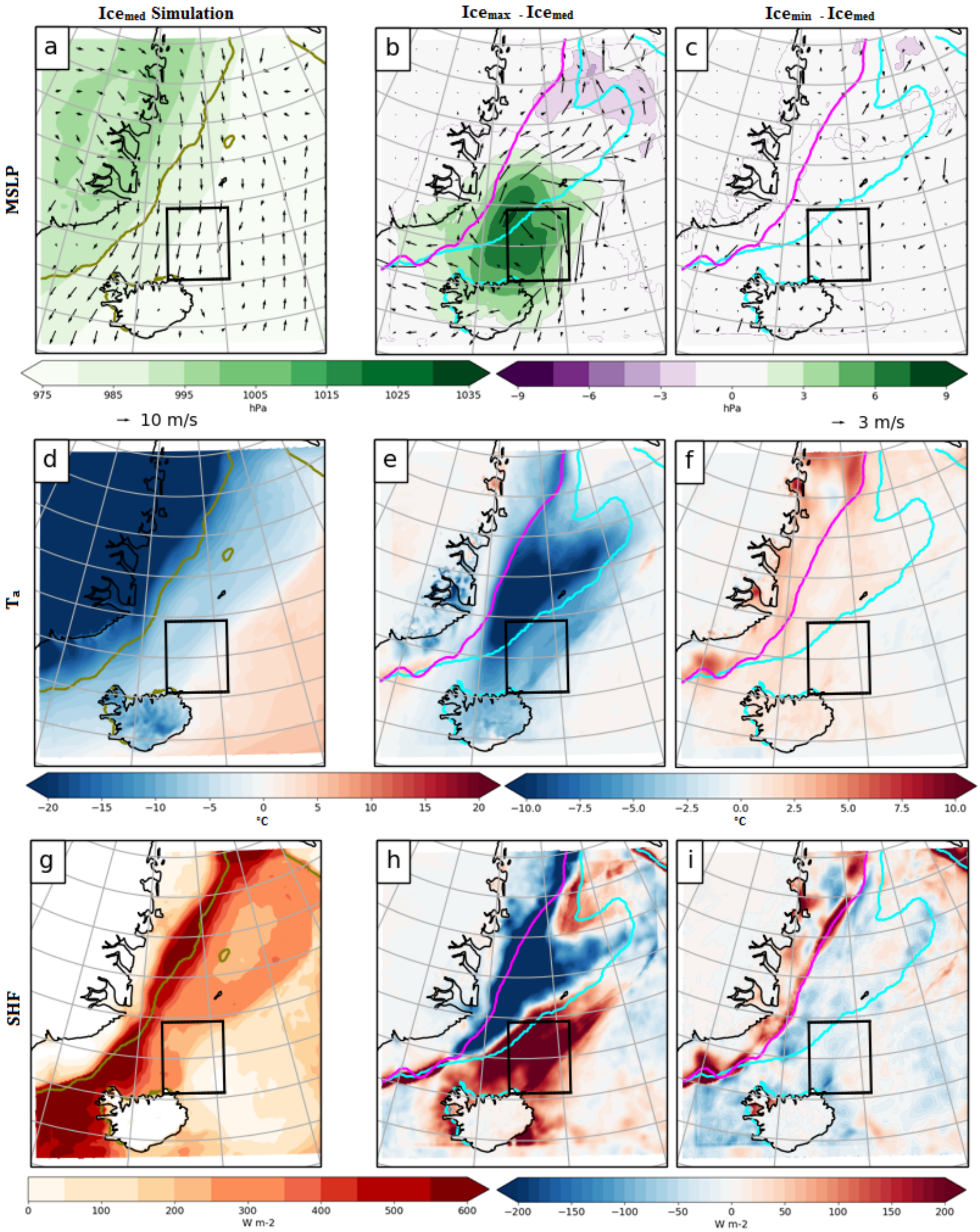

Figure 7 – A case study analysis for the 31st January 1995, a high heat flux event when surface heat fluxes in the Ice$_{max}$ simulation were greater than the Ice$_{min}$ simulation in the Iceland Sea gyre. Mean sea level pressure (MSLP) and 10m wind vectors (units of hPa & ms^{-1} respectively), air temperature at 1.5 m (T$_a$; units of °C) and surface heat flux (SHF; units of W m^{-2}) for the Ice$_{med}$ simulation (a, d & j) and corresponding anomalies for the Ice$_{max}$ - Ice$_{med}$ simulations (b, e & h); and the Ice$_{min}$ - Ice$_{med}$ simulations (c, f & i). The 15% sea-ice concentration contours are selectively plotted: Ice$_{max}$ simulation (cyan), Ice$_{med}$ simulation (olive) and Ice$_{min}$ simulation (magenta).

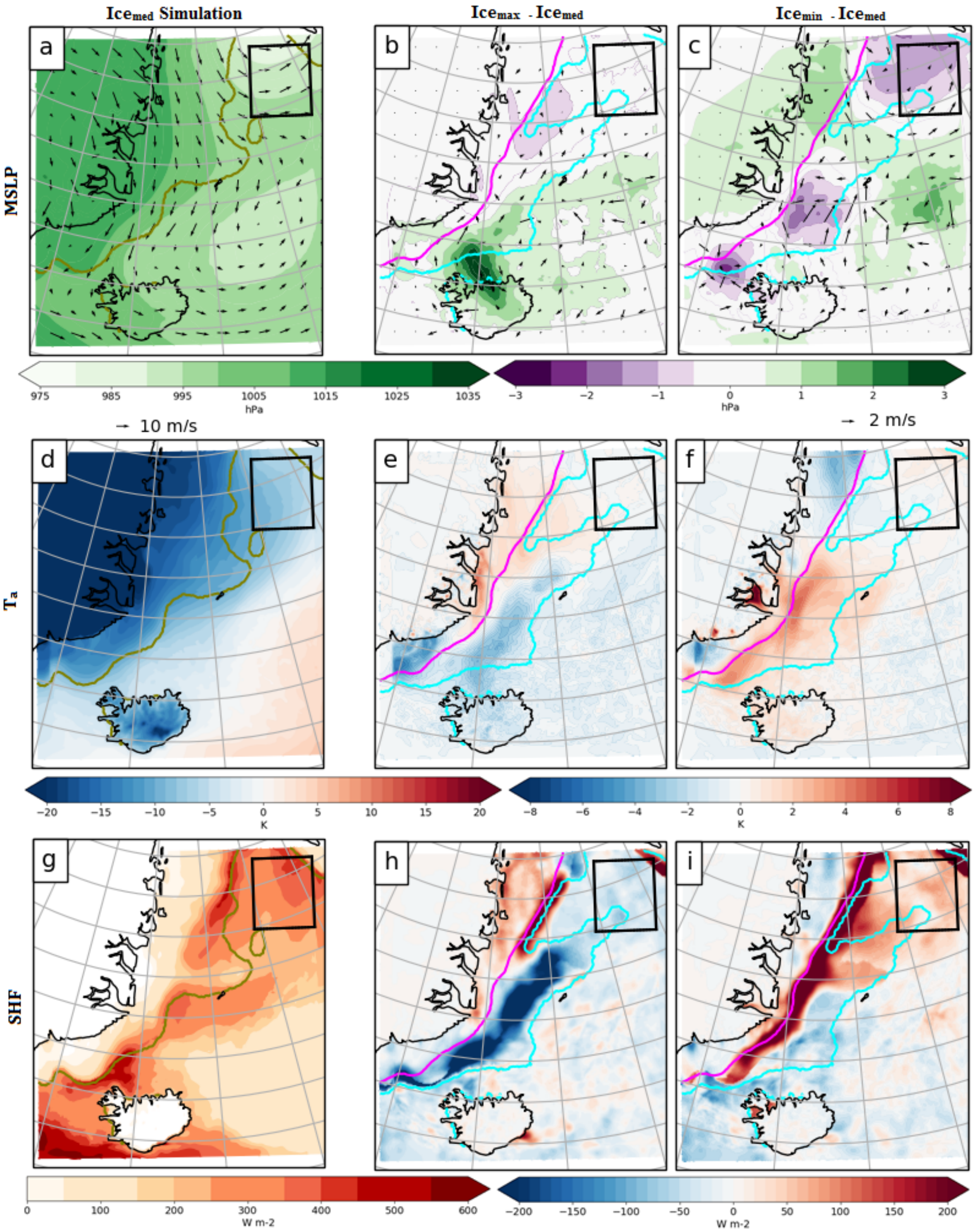

Figure 8 – A case study analysis for the 25th Feb 1993, a high heat flux event when surface heat fluxes in the Ice$_{min}$ simulation were greater than the Ice$_{max}$ simulation in the Greenland Sea gyre. Mean sea level pressure (MSLP) and 10m wind vectors (units of hPa & ms^{-1} respectively), air temperature at 1.5 m (T$_a$; units of °C) and surface heat flux (SHF; units of W m^{-2}) for the Ice$_{med}$ simulation (a, d & j) and corresponding anomalies for the Ice$_{max}$ - Ice$_{med}$ simulations (b, e & h); and the Ice$_{min}$ - Ice$_{med}$ simulations (c, f & i). The 15% sea-ice concentration contours are selectively plotted: Ice$_{max}$ simulation (cyan), Ice$_{med}$ simulation (olive) and Ice$_{min}$ simulation (magenta).

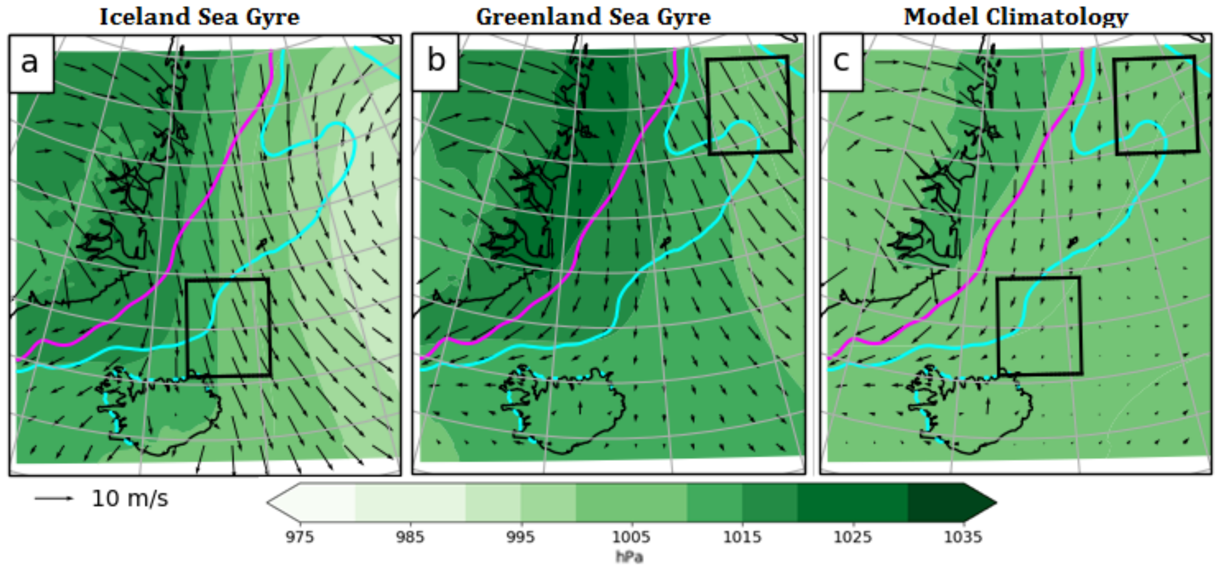

Figure 9 – Composite analysis of mean sea level pressure (MSLP; units of hPa) and 10m wind vectors (units of ms^{-1}) for the occasions of high heat flux events in (a) the Iceland Sea gyre (for the Ice_{max} simulation) and (b) the Greenland Sea gyre (for the Ice_{min} simulation) and (c) the model climatological average (all simulated days). The 15% sea-ice concentration contours are selectively plotted: Ice_{max} simulation (cyan), and Ice_{min} simulation (magenta). The boxes represent the location of the Iceland Sea and the Greenland Sea gyres used in this study.

	Period	Average surface heat flux (W m^{-2})		Differences (Ice_{min} – Ice_{max})	
		Ice_{max}	Ice_{min}	Absolute Anomaly (W m^{-2})	Percentage Anomaly
Iceland Sea Gyre	JFMA	134	115	-19	-15%
	January	150	106	-44	-30%
	February	122	110	-12	-10%
	March	121	114	-7	-6%
	April	104	99	-5	-5%
Greenland Sea Gyre	JFMA	125	134	9	8%
	January	140	153	13	10%
	February	118	132	14	12%
	March	114	123	9	7%
	April	100	113	13	13%

Table 1 - Mean surface heat fluxes for the Ice_{max} and Ice_{min} simulations averaged over the Iceland Sea and Greenland Sea gyres. Means are presented for the winter season (JFMA) and each winter month. The percentage difference between the fluxes is shown in the final column and was calculated as (Ice_{min} - Ice_{max})/Ice_{max}.

	Period	Number high heat flux events	Ice_{max} event > Ice_{min} event
Iceland Sea Gyre	JFMA	177	76%
	January	53	96%
	February	47	74%
	March	39	82%
	April	38	55%
			Ice_{max} event < Ice_{min} event
Greenland Sea Gyre	JFMA	199	93%
	January	51	92%
	February	40	93%
	March	55	93%
	April	53	96%

Table 2 - High heat flux events in the Iceland and Greenland Sea gyres, presented for the winter season (JFMA) and each winter month. Columns show the number of high heat flux events, and the percentage of events where average heat fluxes in Ice_{max} > Ice_{min} (Iceland Sea gyre) or Ice_{max} < Ice_{min} (Greenland Sea gyre).